Anisotropic large diamagnetism in Dirac semimetals $ZrTe_5$ and $HfTe_5$

OPEN ACCESS
IOP Publishing
Journal of Physics: Condensed Matter
J. Phys.: Condens. Matter **34** (2022) 225802 (6pp)
https://doi.org/10.1088/1361-648X/ac5d19

Anisotropic large diamagnetism in Dirac semimetals $ZrTe_5$ and $HfTe_5$

Sukriti Singh, Nitesh Kumar, Subhajit Roychowdhury, Chandra Shekhar* and Claudia Felser

Max Planck Institute for Chemical Physics of Solids, 01187 Dresden, Germany

E-mail: Chandra.Shekhar@cpfs.mpg.de

Received 3 July 2021, revised 16 February 2022
Accepted for publication 11 March 2022
Published 1 April 2022

Abstract

Dirac semimetals, e.g., $ZrTe_5$ and $HfTe_5$, have been widely investigated and have exhibited various exotic physical properties. Nevertheless, several properties of these compounds, including diamagnetism, are still unclear. In this study, we measured the temperature- and field-dependent diamagnetism of $ZrTe_5$ and $HfTe_5$ along all three crystallographic axes (*a*-, *b*-, and *c*-axis). The temperature-dependent magnetization shows an anomaly, which is a characteristic of Dirac crossing. Diamagnetic signal reaches the highest value of 17.3×10^{-4} emu mol^{-1} Oe^{-1} along the van der Waals layers, i.e., the *b*-axis. However, the diamagnetism remains temperature-independent along the other two axes. The field-dependent diamagnetic signal grows linearly without any sign of saturation and maintains a large value along the *b*-axis. Interestingly, the observed diamagnetism is anisotropic like other physical properties of these compounds and is strongly related to the effective mass, indicating the dominating contribution of orbital diamagnetism in Dirac semimetals induced by interband effects. $ZrTe_5$ and $HfTe_5$ show one of the largest diamagnetic value among previously reported state-of-the-art topological semimetals. Our present study adds another important experimental aspect to characterize nodal crossing and search for other topological materials with large magnetic susceptibility.

Keywords: diamagnetism, anisotropy, effective mass, Dirac semimetal

(Some figures may appear in colour only in the online journal)

1. Introduction

Topological quantum materials have attracted considerable attention in condensed matter physics and material science in recent years. Topological quantum materials with various band structure topologies exist, which capture more than 20% compounds of the ICSD database [1]. Among them, semimetals are particularly interesting as their topology can even appear close to the Fermi energy (E_F), which directly influences their physical properties. The degeneracy of band touching in momentum space determines the classification of the topology [2]. In particular, the bands of Dirac semimetals touch at nodes with four-fold degeneracy, known as Dirac point/node, and numerous families of such compounds have been discovered [3]. Transition-metal pentatellurides, namely $ZrTe_5$ and $HfTe_5$, are the most studied topological Dirac semimetal, and they behave as quasi two-dimensional (2D) semimetals owing to the presence of van der Waals coupling between layers [4]. There is a debate about whether these compounds are strong or weak topological insulators, considering that these two phases differ only by the small lattice parameters [5, 6]. The bulk conduction band nearly touches the bulk valence band, forming a bulk Dirac cone, which fit in the criteria of 3D Dirac semimetals with small band gap [7]. $ZrTe_5$ and $HfTe_5$ show many interesting physical properties, including resistivity anomaly [8–10], high mobility [11], chiral anomaly [11], anomalous

* Author to whom any correspondence should be addressed.

Hall effect [12], 3D quantum Hall effect [13–15], low thermal conductivity [16], and large Seebeck coefficients [17]. Owing to the presence of an anisotropic Fermi surface, these properties are very anisotropic and can easily be tuned by applying strain or pressure, which is beneficial for tunable applications [18]. Moreover, both $ZrTe_5$ and $HfTe_5$ shows an anomaly in the temperature-dependent resistivity, at temperature mainly known as the transition temperature T_p, at which the charge carrier type changes [10, 19]. The most feasible explanation of this anomaly is the sweeping of the chemical potential with temperature through the Dirac point [8].

Magnetization of these compounds have never been the part of the investigation along with other physical properties, even though a controversial anomaly is seen in temperature dependence resistivity and thermopower. Usually, the magnetization of 3D Fermi gas exhibits paramagnetic response known as Pauli-spin paramagnetism and diamagnetic response from Larmor diamagnetism and Landau diamagnetism, wherein the paramagnetic response dominates and is approximately three times larger than Landau diamagnetic response [20]. However, Landau (orbital) diamagnetic response can dominate over paramagnetic response, depending on the origins. For example, when the interband effect dominates in the presence of strong spin–orbit coupling, orbital diamagnetism is enhanced [21] and the reasonably high value of diamagnetism was observed in bismuth [22]. The diamagnetism has recently been studied in various semimetals including topological semimetals like graphene, Bi, TaAs, Sr_3PbO, and $Bi_{(1-x)}Sb_x$, where orbital diamagnetism is responsible for such large diamagnetism [23–28]. The spin–orbit coupling is one of the main tuning parameters, and is unavoidably present in the topological semimetals in which a large orbital diamagnetism can be expected. In this regard, we strongly believe that $ZrTe_5$ and $HfTe_5$ are the best suitable candidates and possess only few bands at E_F. The thermodynamic evidence through magnetization of such bands can really be promising, which can also track the movement of chemical potential. Our present study reveals large anisotropic diamagnetism and anomaly in temperature dependence magnetization similar to resistivity and thermopower, and shows how effective mass of charge carriers and position of chemical potential are correlated with the diamagnetism. The anomaly seen in temperature dependence magnetization is characteristics of nodal crossing at which inter band scattering enhances.

Both $ZrTe_5$ and $HfTe_5$ crystallize in orthorhombic crystal structure with space group (SG) *Cmcm* (63), as shown in figure 1(a). In this figure, we can see that van der Waals layers are stacked along the crystallographic *b*-axis, while the prism chains of transition metals surrounded by Te atoms run along the *a*-axis. These prismatic chains are linked by zigzag Te atoms along the *c*-axis, forming a 2D sheet of Zr/$HfTe_5$ in the *a*–*c* plane [4]. These atomic arrangements facilitate the crystal growth in long plate-like shape. The length and cleaving planes are always along the *a*-axis and the *ac*-plane, respectively. Although various interesting properties of $ZrTe_5$ and $HfTe_5$ have been investigated, many more properties, including diamagnetism, are still deceptive. In this study, we investigated the diamagnetism and found it to be -17.33×10^{-4} emu mol^{-1} Oe^{-1} for $ZrTe_5$ and -12.49×10^{-4} emu mol^{-1} Oe^{-1} for $HfTe_5$ at T_p in 1 T, which is highest among the previously reported state-of-the-art topological semimetals [25–27]. An anomaly develops at T_p in temperature-dependent magnetization measurement, which was illusive and now adds an important experimental aspect characterizing nodal crossing. The highest diamagnetic signal appears at T_p. Measured diamagnetic signal is sensitive to the band structure and the position of chemical potential specifically when topological nodes are present near to the E_F.

2. Experimental details

Zr/$HfTe_5$ crystals were synthesized by chemical vapor transport following a previously reported method [17]. The magnetic measurements were performed using a superconducting quantum interference device vibrating sample magnetometer (MPMS 3, Quantum Design) with a sensitivity of 10^{-7} emu. For minimizing the error in the measurements, we used the same quartz paddle holder for every measurement with the same amount of adhesive tape to stick the sample to the quartz paddle, instead of using GE varnish. A background measurement was taken for the quartz paddle with adhesive tape and was subtracted from each measurement with the sample. The field as well as temperature-dependent magnetization for Zr/$HfTe_5$ were measured over a magnetic field range of -7 to $+7$ T at temperatures between 2 and 300 K with field along all three crystallographic axes.

3. Results and discussion

It has been known that $ZrTe_5$ and $HfTe_5$ are electronically quasi-2D, and it is more interesting to see whether this behavior also retains when subjected to a magnetic field. To this end, we measured the temperature-dependent magnetization *M* along different axes at various magnetic field intensities. Figures 1(b) and (c) show plots of the magnetization along the *b*-axis at a fixed magnetic field intensity of 1 T and the zero-field resistivity along the *a*-axis of $ZrTe_5$ and $HfTe_5$, respectively. Both the compounds exhibit diamagnetic signals over the entire temperature range. The magnitude of *M* continuously increases with temperature and shows a deep minimum at 130 and 65 K for $ZrTe_5$ and $HfTe_5$, respectively; as the temperature lower further, the magnitude of *M* decreases. The above mentioned temperatures correspond to their respective temperature T_p at which anomaly appear in the resistivity also, wherein charge carrier changes sign in Hall resistivity [17]. The minimum in the curve corresponds to the highest diamagnetic value of -17.33 and -12.44 emu mol^{-1} for $ZrTe_5$ and $HfTe_5$, respectively, at an applied magnetic field of 1 T. The resistivity anomaly peaks observed in figures 1(b) and (c) correspond to 3.7 and 60 mΩ cm at T_p in $ZrTe_5$ and $HfTe_5$, respectively; the anomaly peak in the temperature-dependent resistivity matches well with the minima observed in temperature-dependent magnetization. Such anomaly was also observed in the thermopower, wherein the Seebeck coefficient changes sign [8, 17].

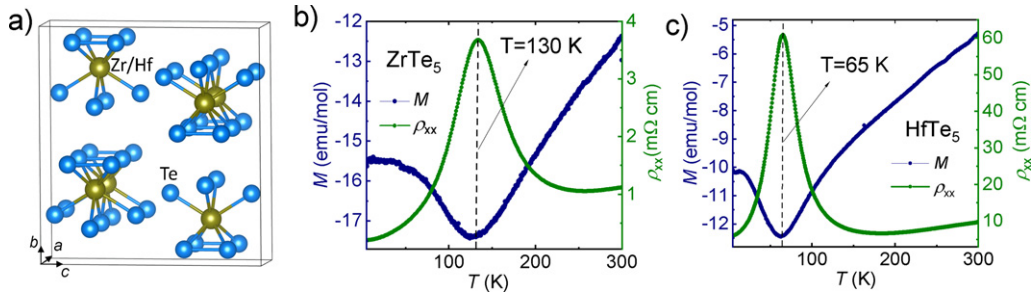

Figure 1. (a) Orthorhombic crystal structure of Zr/$HfTe_5$, showing that the layers are stacked along the *b*-axis where van der Waals layers are present. Temperature-dependent zero field longitudinal resistivity ρ_{xx} along *a*-axis and magnetization *M* along crystallographic *b*-axis measured at magnetic field *B* of 1 T for (b) $ZrTe_5$ and (c) $HfTe_5$. The dotted lines correspond to the anomaly transition temperature T_p.

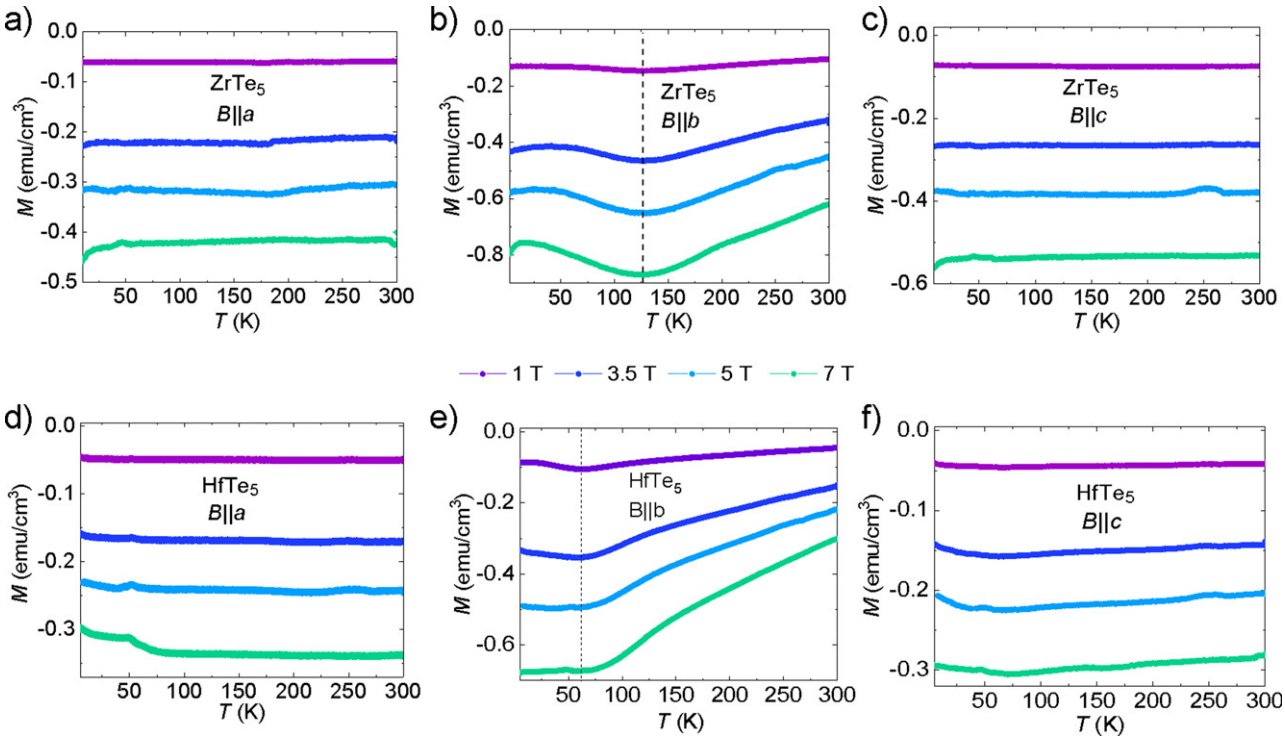

Figure 2. Temperature dependence of the magnetization *M* at different applied magnetic fields along (a) *a*-, (b) *b*-, and (c) *c*-axes for $ZrTe_5$ and along (d) *a*-, (e) *b*-, and (f) *c*-axes for $HfTe_5$. In both (b) and (e) an anomaly is observed, similar to that observed in the resistivity and thermopower; the dotted line corresponds to T_p.

Figure 2 shows plots of the temperature-dependent magnetization for $ZrTe_5$ and $HfTe_5$ along all three crystallographic axes at field intensities of 1, 3.5, 5 and 7 T. It can be seen that when the field is along the *a*- and *c*-axes, the magnetization is almost temperature independent throughout the measured temperature range at fixed field. However, when the applied field is along the *b*-axis, the magnetization shows significant temperature dependence. We observe a linear decrease in magnetization with lowering temperature until T_p, above which the magnetization increases slightly while approaching the lowest temperature. Such temperature-dependent magnetization can be interpreted in terms of change in chemical potential through the Dirac point. In figures 2(b) and (e), the behavior of temperature dependent magnetization curve below from T_p is slightly different when intensity of field is increased. The probable reason behind this is that, in $ZrTe_5$ the Fermi surface spectral width is higher for electron pocket as paramagnetic signal and thus responsible for the upturn, decreasing the strength of diamagnetic signal while in case of $HfTe_5$ it is just opposite i.e. hole pocket spectral width is higher contributing in diamagnetic signal [10]. The small kink in the magnetizations around 50 K is rather known and is due to the presence of O_2 molecule in the chamber.

In particular, for $ZrTe_5$, the value of *M* at 7 T along the *b*-axis is -0.81 emu cm^{-3} at 2 K, and it reaches the maximum value of -0.87 emu cm^{-3} at T_p (130 K). A further decrease in diamagnetism is observed at 300 K, with a value of -0.62 emu cm^{-3} at 300 K. The same trend is observed

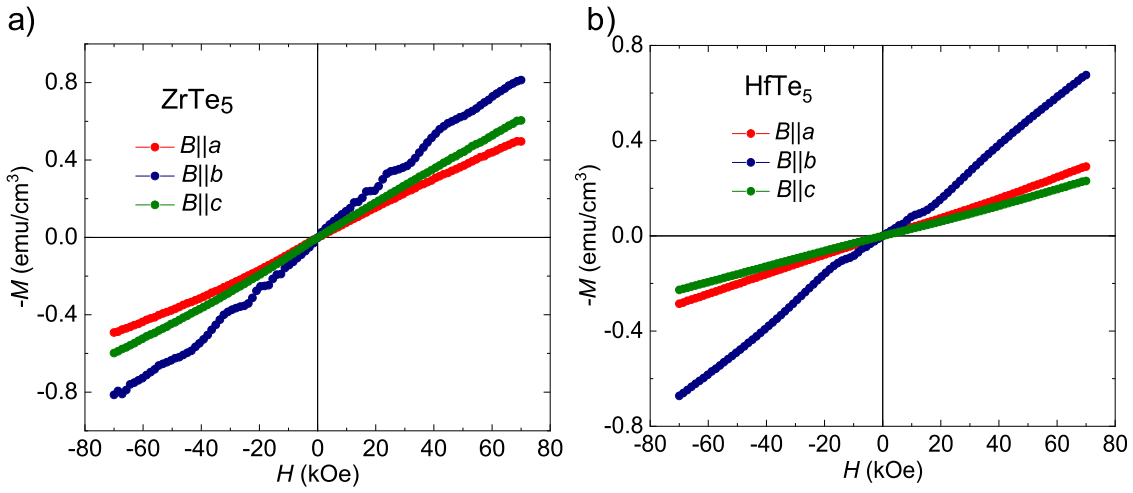

Figure 3. Field-dependent isothermal magnetization measured in range of +7 to −7 T at 2 K along all three crystallographic axes for (a) $ZrTe_5$ and (b) $HfTe_5$. The highest diamagnetization is reached along the *b*-axis.

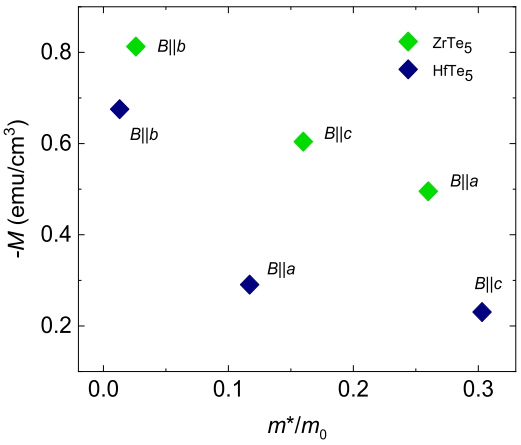

Figure 4. Correlation between magnetization *M* and effective mass m^*. The diamagnetic signal decreases as effective mass increases and is highest along the *b*-axis wherein the effective mass is the lowest.

for $HfTe_5$, with slightly lower diamagnetic values. For $HfTe_5$, the values of *M* along the *b*-axis at 7 T are −0.60, −0.68, and −0.29 emu cm^{-3} at 2 K, T_p (65 K), and 300 K, respectively.

We measured the isothermal magnetization for $ZrTe_5$ and $HfTe_5$ at temperatures between 2 to 300 K; for simplicity, we only report the magnetization measured at 2 K along all crystallographic axes (figures 3(a) and (b)). The isothermal magnetization at 2 K and 7 T for $ZrTe_5$ along the *a*-, *b*-, and *c*-axes are −0.49, −0.81, and −0.60 emu cm^{-3}, respectively. In the same conditions, the magnetization of $HfTe_5$ when *B* is along the *a*-, *b*-, and *c*-axes is −0.29, −0.68, and −0.23 emu cm^{-3}, respectively. Besides these high magnetization values, the diamagnetic signal also comprises quantum oscillations, which start below 1 T proving the high quality of crystals. It is true that the quantum oscillations appear in magnetization only along *b*-axis, and other two axes do not show. However, these oscillations are present along all the axes in resistivity [14, 15]. Usually, the sensitivity of the measurement types depends on the shape of Fermi surface for example, magnetization is sensitive to asymmetrical Fermi surface while resistivity for symmetrical. If the Fermi surface is asymmetrical in a sense that extremal area normal to applied field varies with the direction of field, there will be torque on the crystal and therefore magnetic measurements are more sensitive for asymmetrical Fermi surface [29]. Different diamagnetic values are observed along different axes within the compound, indicating anisotropic behavior, which is relatively high in $HfTe_5$. Here, we correlate the observed anisotropic magnetization with the anisotropic effective mass. The anisotropic effective mass m^* for $ZrTe_5$ along the *a*-, *b*-, and *c*-axes is $0.26m_0$, $0.026m_0$, and $0.16m_0$, respectively, where m_0 is the bare mass of an electron, and the corresponding values for $HfTe_5$ are $0.117m_0$, $0.013m_0$, and $0.303m_0$, respectively [15, 30]. Figure 4 shows a plot of the magnetization as a function of the effective mass. From the figure, it can be seen that the smaller effective mass exhibits comparatively larger diamagnetism. This correlation can be attributed to the fact that the Landau diamagnetism (χ_{LD}) dominates over the Pauli spin paramagnetism (χ_{PP}) if the effective mass is very small as $\chi_{LD}/\chi_{PP} \sim (m_0/m^*)^2$ [20] which illustrates that the small effective mass enhances the orbital diamagnetic signal. The anisotropic effective mass ratio for $HfTe_5$ $(m_c^*/m_b^*)^2$ and $ZrTe_5$ $(m_a^*/m_b^*)^2$ is approximately 550 and 100, respectively, which explains the relatively larger anisotropy found in $HfTe_5$ compared to that in $ZrTe_5$. Here, we selected the effective mass along the *a*-axis instead of the *c*-axis for $ZrTe_5$ to show the highest anisotropy.

Recently, high orbital diamagnetism was observed in several topological semimetals with linear dispersion near the E_F, e.g., TaAs, $Bi_{0.92}Sb_{0.08}$, $Bi_{0.84}Sb_{0.16}$, and Sr_3PbO [25, 27, 28, 31]. From figure 5, we can see that $ZrTe_5$ and $HfTe_5$ shows one the largest magnetic susceptibility (*M*/*H*) among previously reported topological semimetals.

In nonmagnetic compounds such as $ZrTe_5$ and $HfTe_5$, magnetism mainly arises from the Pauli paramagnetism, and Landau diamagnetism. The former one is induced by the spin of the

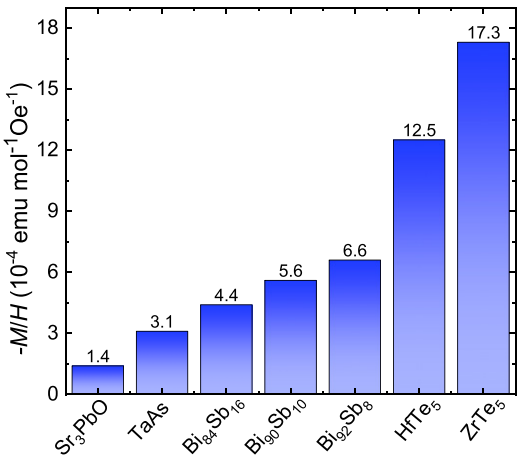

Figure 5. Histogram showing M/H values for previously reported topological semimetals, where $ZrTe_5$ and $HfTe_5$ (present work) shows one of the largest values reported till yet [24, 26–28].

free electrons, while the latter one originates from the orbital motion. In addition to these two, the Larmor diamagnetism also contributes in diamagnetism which originates from core ions, but it is magnitude is normally very small. In particular case of $ZrTe_5$ and $HfTe_5$, the contribution from Larmor diamagnetism is found to be 8.0×10^{-5} emu mol^{-1} Oe^{-1} and 8.6×10^{-5} emu mol^{-1} Oe^{-1}, respectively. While the experimentally observed value is of order 10^{-3} emu mol^{-1} Oe^{-1} which is two order of magnitude higher, clearly indicating a large contribution from the orbital diamagnetism. For any 3D isotropic Dirac system, value of orbital magnetic susceptibility $\chi = \frac{e^2 v_f}{\pi^2 \hbar c^2} \ln\left(\frac{2E_c}{\Delta}\right)$, where e is elementary charge, $\hbar$ is reduced Planck constant, c is speed of light, E_c is cutoff energy, v_f is Fermi velocity and Δ is gap [32]. The susceptibility depends on Fermi velocity v_f and gap Δ, if interband effects are taken into consideration [32, 33]. Interband transition is more feasible if the band gap is small, thus enhancing the orbital diamagnetism. After taking the naively values of $\Delta = 10$ meV [19], $v_{fa} = 1.7 \times 10^5$ m s^{-1}, $v_{fb} = 5.2 \times 10^5$ m s^{-1}, $v_{fc} = 2.2 \times 10^5$ m s^{-1} [30] for $ZrTe_5$; and $\Delta = 10$ meV [10], $v_{fa} = 1.7 \times 10^5$ m s^{-1}, $v_{fb} = 6.4 \times 10^5$ m s^{-1}, $v_{fc} = 0.8 \times 10^5$ m s^{-1} [15] for $HfTe_5$, considering the system isotropic and $E_c = 500$ meV in the above relation, the value of magnetization at 7 T for $ZrTe_5$ along a-, b- and c-axes is 0.14, 0.41 and 0.17 emu cm^{-3} respectively, and for $HfTe_5$ along a, b and c-axes is 0.14, 0.51 and 0.06 emu cm^{-3}. The magnitude of magnetic susceptibility merely changes even if we change E_c by a large amount [34]. These values are of the order as measured values depicting huge enhancement in diamagnetism from orbital diamagnetism.

We observed unusual large diamagnetism along the b-axis, along which the diamagnetism is highly temperature-dependent, while along other two axes, it is almost temperature-independent. In a previous study, large diamagnetism was observed in Bi wherein the interband scattering effect was considered, which enhances the orbital diamagnetism when E_F lies between the gap [21, 24]. Similarly, in our study, we also observed that the highest diamagnetic signal corresponding to T_p occurred when the chemical potential lied between the gap [35]. However, an additional factor also controls the diamagnetism. The most likely factor is the anisotropic effective mass according to Landau diamagnetism, as mentioned above. Among all the axes, the effective mass is the smallest along b-axis, where van der Waals coupling exists between the layers, and the diamagnetic signal is highest. For the Dirac dispersion, the effective mass does not change with energy, in contrast to the case of parabolic dispersion. Considering the fact that $ZrTe_5$ and $HfTe_5$, the dispersion along the a- and c-axes is linear, while such linear dispersion is suppressed by a parabolic component along the b-axis [36, 37]. We observed nearly temperature-independent diamagnetic signals along the a- and c-axes. However, the diamagnetic signal changes with temperature along the b-axis, along which the effective mass is expected to change. Therefore, the diamagnetic signal measured in this study are consistent with the anisotropic dispersion of the bulk Dirac cone, which results in an anisotropic effective mass. Such a strong correlation between the effective mass and magnetization clearly indicate that the orbital contribution is dominant.

4. Conclusion

We measured the one of the largest magnitudes of diamagnetism in $ZrTe_5$ and $HfTe_5$ among previously reported topological semimetals. The magnetization measured is very anisotropic and temperature-independent along the a- and c-axes. Along the b-axis, they have anomalous behavior similar to that of the resistivity and thermopower observed in previous studies. The highest diamagnetic signal was observed at T_p, at which the chemical potential lies in the gap. Within the different axes, the b-axis shows the highest diamagnetism, which is in accordance with the lower effective mass compared to that in the other axes, indicating the dominant role of orbital diamagnetic contribution. Our study adds another physical property as giant diamagnetism to other known physical properties in $ZrTe_5$ and $HfTe_5$, motivating others to look for topological semimetals resulting in such large diamagnetism. This work also provides a thermodynamic experimental platform to investigate nodal crossing.

Acknowledgments

This work was financially supported by Deutsche Forschungsgemeinschaft (DFG) under SFB 1143 (Project No. 247310070), the European Research Council (ERC) Advanced Grant No. 742068 ('TOPMAT'), and Würzburg-Dresden Cluster of Excellence on Complexity and Topology in Quantum Matter—ct.qmat (EXC 2147, Project No. 39085490). SR thanks the Alexander von Humboldt Foundation for a fellowship.

Data availability statement

All data that support the findings of this study are included within the article (and any supplementary files).

ORCID iDs

Sukriti Singh https://orcid.org/0000-0003-0231-8445
Chandra Shekhar https://orcid.org/0000-0002-3330-0400

References

[1] Gibney E 2018 Thousands of exotic 'topological' materials discovered through sweeping search *Nature* **560** 151
[2] Yan B and Felser C 2017 Topological materials: Weyl semimetals *Annu. Rev. Condens. Matter Phys.* **8** 337–54
[3] Armitage N P, Mele E J and Vishwanath A 2018 Weyl and Dirac semimetals in three-dimensional solids *Rev. Mod. Phys.* **90** 015001
[4] Yang P, Wang W, Zhang X, Wang K, He L, Liu W and Xu Y 2019 Quantum oscillations from nontrivial states in quasi-two-dimensional Dirac semimetal $ZrTe_5$ nanowires *Sci. Rep.* **9** 3558
[5] Weng X, Dai X and Fang Z 2014 Transition-metal pentatelluride $ZrTe_5$ and $HfTe_5$: a paradigm for large-gap quantum spin Hall insulators *Phys. Rev.* X **4** 011002
[6] Manzoni G *et al* 2016 Evidence for a strong topological insulator phase in $ZrTe_5$ *Phys. Rev. Lett.* **117** 237601
[7] Xiong H *et al* 2017 Three-dimensional nature of the band structure of $ZrTe_5$ measured by high momentum-resolution photoemission spectroscopy *Phys. Rev.* B **95** 195119
[8] Fu B, Wang H W and Shen S Q 2020 Dirac polarons and resistivity anomaly in $ZrTe_5$ and $HfTe_5$ *Phys. Rev. Lett.* **125** 256601
[9] Okada S, Sambongi T and Ido M 1980 Giant resistivity anomaly in $ZrTe_5$ *J. Phys. Soc. Japan* **49** 839
[10] Zhang Y *et al* 2017 Temperature-induced Lifshitz transition in topological insulator candidate $HfTe_5$ *Sci. Bull.* **62** 950
[11] Wang H *et al* 2016 Chiral anomaly and ultrahigh mobility in crystalline $HfTe_5$ *Phys. Rev.* B **93** 165127
[12] Liu Y *et al* 2021 Induced anomalous Hall effect of massive Dirac fermions in $ZrTe_5$ and $HfTe_5$ thin flakes *Phys. Rev.* B **103** L201110
[13] Galeski S *et al* 2021 Origin of the quasi-quantized Hall effect in $ZrTe_5$ *Nat. Commun.* **12** 3197
[14] Tang F *et al* 2019 Three-dimensional quantum Hall effect and metal–insulator transition in $ZrTe_5$ *Nature* **569** 537
[15] Galeski S *et al* 2020 Unconventional Hall response in the quantum limit of $HfTe_5$ *Nat. Commun.* **11** 5926
[16] Zhu J, Feng T, Mills S, Wang P, Wu X, Zhang L, Pantelides S T, Du X and Wang X 2018 Record-low and anisotropic thermal conductivity of a quasi-one-dimensional bulk $ZrTe_5$ single crystal *ACS Appl. Mater. Interfaces* **10** 40740
[17] Shahi P *et al* 2018 Bipolar conduction as the possible origin of the electronic transition in pentatellurides: metallic vs semiconducting behavior *Phys. Rev.* X **8** 021055
[18] Mutch J, Chen W C, Went P, Qian T, Wilson I Z, Andreev A, Chen C C and Chu J H 2019 Evidence for a strain-tuned topological phase transition in $ZrTe_5$ *Sci. Adv.* **5** eaav977
[19] Zhang Y *et al* 2017 Electronic evidence of temperature-induced Lifshitz transition and topological nature in $ZrTe_5$ *Nat. Commun.* **8** 15512
[20] Ashcroft N W and Mermin N D 1976 *Solid State Physics* 1st edn ed D G Crane (New York: Hartcourt College Publishers) p 666
[21] Fukuyama H and Kubo R 1970 Interband effects on magnetic susceptibility: II. Diamagnetism of bismuth *J. Phys. Soc. Japan* **28** 570–81
[22] Otake S, Momiuchi M and Matsuno N 1980 Temperature dependence of the magnetic susceptibility of bismuth *J. Phys. Soc. Japan* **49** 1824–8
[23] Li Z, Chen L, Meng S, Guo L, Huang J, Liu Y, Wang W and Chen X 2015 Field and temperature dependence of intrinsic diamagnetism in graphene: theory and experiment *Phys. Rev.* B **91** 094429
[24] Fuseya Y, Ogata M and Fukuyama H 2014 Transport properties and diamagnetism of Dirac electrons in bismuth *J. Phys. Soc. Japan* **84** 012001
[25] Liu Y, Prucnal S, Zhou S, Li Z, Guo L, Chen X, Yuan Y, Liu F and Helm M 2016 Intrinsic diamagnetism in the Weyl semimetal TaAs *J. Magn. Magn. Mater.* **408** 73–6
[26] Zhang C L *et al* 2019 Non-saturating quantum magnetization in Weyl semimetal TaAs *Nat. Commun.* **10** 1028
[27] Suetsugu S, Kitagawa K, Kariyado T, Rost A W, Nuss J, Mühle C, Ogata M and Takagi H 2021 Giant orbital diamagnetism of three-dimensional Dirac electrons in Sr_3PbO antiperovskite *Phys. Rev.* B **103** 115117
[28] Watanabe Y, Kumazaki M, Ezure H, Sasagawa T, Cava R, Itoh M and Shimizu Y 2021 Local observations of orbital diamagnetism and excitation in three-dimensional Dirac fermion systems $Bi_{1-x}Sb_x$ *J. Phys. Soc. Japan* **90** 053701
[29] Shoenberg D 1984 *Magnetic Oscillations in Metals* (Cambridge: Cambridge University Press) p 87
[30] Liu Y *et al* 2016 Zeeman splitting and dynamical mass generation in Dirac semimetal $ZrTe_5$ *Nat. Commun.* **7** 12516
[31] Shoenberg D and Uddin M Z 1936 The magnetic properties of bismuth: II. The de Haas–van Alphen effect *Proc. R. Soc.* A **156** 701–20
[32] Koshino M and Ando T 2010 Anomalous orbital magnetism in Dirac-electron systems: role of pseudospin paramagnetism *Phys. Rev.* B **81** 195431
[33] Fuseya Y, Ogata M and Fukuyama H 2012 Spin-Hall effect and diamagnetism of Dirac electrons *J. Phys. Soc. Japan* **81** 093704
[34] Fuseya Y, Ogata M and Fukuyama H 2014 Spin-Hall effect and diamagnetism of anisotropic Dirac electrons in solids *J. Phys. Soc. Japan* **83** 074702
[35] Tian Y, Ghassemi N and Ross J H Jr 2019 Dirac electron behavior and NMR evidence for topological band inversion in $ZrTe_5$ *Phys. Rev.* B **100** 165149
[36] Jiang Y *et al* 2020 Unraveling the topological phase of $ZrTe_5$ via magnetoinfrared spectroscopy *Phys. Rev. Lett.* **125** 046403
[37] Martino E *et al* 2019 Two-dimensional conical dispersion in $ZrTe_5$ evidenced by optical spectroscopy *Phys. Rev. Lett.* **122** 217402